Particle
& Particle Systems Characterization

Postfach 10 11 61
69451 Weinheim
Germany
Courier services:
Boschstraße 12
69469 Weinheim
Germany
Tel.: (+49) 6201 606 234
Fax: (+49) 6201 606 500
E-mail: particle@wiley.com

WILEY-VCH

Dear Author,

Please correct your galley proofs carefully and return them no more than four days after the page proofs have been received.

Please limit corrections to errors already in the text; cost incurred for any further changes or additions will be charged to the author, unless such changes have been agreed upon by the editor.

The editors reserve the right to publish your article without your corrections if the proofs do not arrive in time.

Note that the author is liable for damages arising from incorrect statements, including misprints.

Please note any queries that require your attention. These are indicated with a Q in the PDF and a question at the end of the document.

Reprints may be ordered by filling out the accompanying form.

Return the reprint order form by fax or by e-mail with the corrected proofs, to Wiley-VCH : particle@wiley.com

To avoid commonly occurring errors, **please ensure that the following important items are correct** in your proofs (please note that once your article is published online, no further corrections can be made):

- **Names** of all authors present and spelled correctly
- **Titles** of authors correct (Prof. or Dr. only: please note, Prof. Dr. is not used in the journals)
- **Addresses** and **postcodes** correct
- **E-mail address** of corresponding author correct (current email address)
- **Funding bodies** included and grant numbers accurate
- **Title** of article OK
- All **figures** included
- **Equations** correct (symbols and sub/superscripts)

Corrections should be made directly in the PDF file using the PDF annotation tools. If you have questions about this, please contact the editorial office. The corrected PDF and any accompanying files should be uploaded to the journal's Editorial Manager site.

Photocatalytic CO_2 Reduction

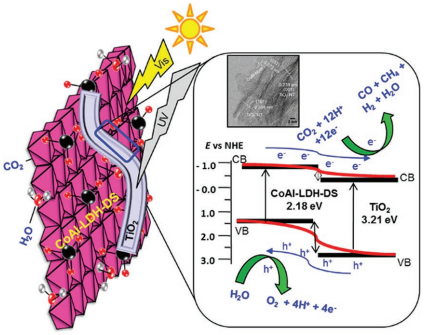

Heterojunction nanocomposites formed between visible and UV light absorbing Co-Al layered double hydroxide and anatase semiconductor nanostructures respectively are efficient photocatalysts for CO_2 reduction under solar irradiation without requiring sacrificial agents.

Particle & Particle Systems Characterization

www.particle-journal.com

Delaminated CoAl-Layered Double Hydroxide@ TiO_2 Heterojunction Nanocomposites for CO_2 Photocatalytic Reduction

*Santosh Kumar, Lee J. Durndell, Jinesh C. Manayil, Mark A. Isaacs, Christopher M. A. Parlett, Sekar Karthikeyan, Richard E. Douthwaite, Ben Coulson, Karen Wilson, and Adam F. Lee**

Photocatalytic reduction offers an attractive route for CO_2 utilization as a chemical feedstock for solar fuels production but remains challenging due to the poor efficiency, instability, and/or toxicity of current catalyst systems. Delaminated CoAl-layered double hydroxide nanosheets (LDH-DS) combined with TiO_2 nanotubes (NTs) or nanoparticles (NPs) are promising nanocomposite photocatalysts for CO_2 reduction. Heterojunction formation between visible light absorbing delaminated CoAl nanosheets and UV light absorbing TiO_2 nanotubes greatly enhances interfacial contact between both high aspect ratio components relative to their bulk counterparts. The resulting synergic interaction confers a significant improvement in photoinduced charge carrier separation, and concomitant aqueous phase CO_2 photocatalytic reduction, in the absence of a sacrificial hole acceptor. CO productivity for a 3 wt% LDH-DS@TiO_2-NT nanocomposite of 4.57 μmol g_{cat}^{-1} h^{-1} exhibits a tenfold and fivefold increase over that obtained for individual TiO_2 NT and delaminated CoAl-LDH components respectively and is double that obtained for 3 wt% bulk-LDH@TiO_2-NT and 3 wt% LDH-DS@TiO_2-NP catalysts. Synthesis of delaminated LDH and metal oxide nanocomposites represents a cost-effective strategy for aqueous phase CO_2 reduction.

1. Introduction

Artificial photosynthesis as a route to solar fuels from CO_2 and water represents a promising strategy to deliver syngas and hydrocarbons as sustainable feedstocks to support global energy needs and security, and (albeit to a limited extent) mitigate anthropogenic climate change.[1,2] Semiconductor nanostructures are promising inorganic mimics of biological photocatalysts in this regard, offering diverse and tunable photophysical and electronic properties.[3–5] Titania is the best known and most widely studied inorganic photocatalyst due to its abundance and low cost, photostability, established redox chemistry, UV absorption, and low toxicity.[6] However, due to the wide band gap of pure titania and extensive recombination of photoexcited charge carriers, various strategies have been exploited to improve its photophysical properties including doping[7] and heterojunction formation,[8] which offer enhanced hydrogen generation[9] and CO_2 reduction.[10] The development of photocatalytic systems with suitable redox behavior to drive solar fuels production remains challenging,[11,12] with the majority of research involving titania systems requiring either a redox mediator[13] or an sacrificial electron/hole scavengers[14] and hence lowering the atom efficiency. Scalable solar fuels production requires low cost and stable materials able to catalyze both photochemical redox reactions without additional reagents.[15] Photocatalytic CO_2 reduction is also problematic due to its poor solubility in aqueous systems and the weak affinity of many inorganic semiconductors.[16]

A range of low dimensional, layered, porous, and/or hybrid inorganic nanomaterials have been investigated for photocatalytic CO_2 reduction, with the primary goal being improved charge carrier separation and transport characteristics and/or morphology, and hence apparent quantum yields and activity[3,4,10] Layered double hydroxides (LDHs) have emerged as promising photocatalysts for CO_2 photoreduction due to their tunable band gap (spanning the UV to visible region), high CO_2 adsorption capacity, relative ease of scale-up, nanoporous architecture, fabrication from earth abundant elements, and conduction and valence energies amenable for driving both CO_2 reduction and water oxidation.[17–19] The first application of a zinc-copper-Al or Ga (III)-LDH[18] for CO_2 photocatalytic reduction found CO and methanol, and various LDHs have

Dr. S. Kumar, Dr. L. J. Durndell, Dr. J. C. Manayil, Dr. M. A. Isaacs, Dr. C. M. A. Parlett, Dr. S. Karthikeyan, Prof. K. Wilson, Prof. A. F. Lee
European Bioenergy Research Institute
Aston University
Birmingham B4 7ET, UK
E-mail: a.f.lee@aston.ac.uk
Dr. R. E. Douthwaite, B. Coulson
Department of Chemistry
University of York
York YO10 5DD, UK
The ORCID identification number(s) for the author(s) of this article can be found under https://doi.org/10.1002/ppsc.201700317.

DOI: 10.1002/ppsc.201700317

been subsequently explored spanning divalent metal cations, such as Mg, Co, Ni, and Zn, and trivalent cations such as Al, In, Ga, and Cr within their interlayers.[19] NiIn-LDHs are the most promising to date for aqueous phase CO_2 photocatalytic reduction to CO, with a productivity of 3.6 μmol g^{-1} h^{-1} under UV light,[17] while defective ZnAl-LDHs are effective for vapor phase CO_2 reduction to CO under UV irradiation.[20] However, pristine LDHs generally exhibit poor quantum efficiency under solar irradiation due to slow charge carrier mobility and high rates of electron–hole recombination.[19] Strategies to improve LDH performance include the use of noble metal (Pt, Pd, and Au)[21] cocatalysts as electron acceptors, or their combination with wide band gap semiconductors[22] to improve utilization of the solar spectrum and/or charge separation. Titania is a good acceptor of photoexcited electrons,[23] and the valence band maximum (VBM)[24] potential of certain LDH materials[25] lies above that of titania (and are hence able to accept photoexcited holes from the latter) yet at an energy sufficient to overcome the overpotential for water oxidation (0.653 eV[26]). We therefore recently synthesized a nanocomposite photocatalyst for aqueous CO_2 photocatalytic reduction, comprising commercial P25 titania in contact with a CoAl-LDH. This exhibited promising activity (2.2 μmol g^{-1} h^{-1}) and >80% selectivity to CO, without requiring a sacrificial hole scavenger.[27] The superior performance of this type-II heterojunction photocatalyst was attributed to increased photoexcited charge carrier lifetimes relative to its individual UV and visible light absorbing semiconductor components, attributed to the spatial separation of charge carriers due to electron transfer from CoAl-LDH → P25, and concomitant hole transfer from P25 → CoAl-LDH, and extended utilization of the solar spectrum. Optimizing the heterojunction interface between titania and LDH components should afford a facile means to further improve photocatalytic performance following rational design principles (such as maximizing the interfacial contact area).

Here, the preceding design strategy is extended through the synthesis of new heterojunction nanocomposites comprising delaminated CoAl-LDH nanosheets dispersed within matrices of high aspect TiO_2 nanoparticles (NPs) or nanotubes (NTs). These nanocomposites enable decoupling of the relative importance of the dimensions/morphology of the visible light (hole-driven) CoAl-LDH[27,28] and UV light (electron-driven) TiO_2 semiconductors[8,27] on CO_2 photocatalytic reduction. CoAl-LDH thickness and titania morphology both strongly influence aqueous CO_2 reduction, with the combination of delaminated CoAl-LDH nanosheets with TiO_2 nanotubes delivering 4.57 (2.0) μmol g_{cat}^{-1} h^{-1} of CO and 0.41 (0.1) μmol g_{cat}^{-1} h^{-1} of CH_4 under UV–vis (visible) irradiation, through a stoichiometric redox process and in the absence of sacrificial agents.

2. Results and Discussion

2.1. Structural Properties of CoAl-LDH and TiO_2 Components

The synthesis of parent CoAl-LDH and TiO_2 nanostructures is summarized in Scheme S1 in the Supporting Information. Powder X-ray diffraction (XRD) of the parent CoAl-LDH and CoAl-LDH-DS materials shown in Figure S1a in the Supporting Information confirmed that both exhibited (d_{00n}) reflections characteristic of the desired layered double hydroxide (JCPDF No. 51-0045). However, the intensity of the (d_{00n}) reflections was significantly suppressed in the delaminated material indicating a loss of long range order and delamination along the (d_{00n}) planes, while the (d_{012}) peak intensity remained similar to the parent LDH indicating that intralayer crystallinity was retained. The interlayer spacing of the parent CoAl-LDH was 0.84 nm (determined from the d_{003} reflection), consistent with the presence of interlayer NO_3^{2-} anions and water.[29] ICP-OES confirmed that the Co:Al stoichiometry was ≈2:1 ratio for both parent and delaminated materials (Table S1, Supporting Information). Note that delamination of CoAl-LDH containing interlayer nitrate anions upon hydrothermal treatment has been previously reported,[29] in contrast to the behavior observed for more stable CoAl-LDH containing interlayer carbonate anions. This stability difference is ascribed to the lower crystallinity of LDH materials prepared with interlayer nitrate versus carbonate anions, which makes assist in deconstructing the former. Our previous study on nanocomposites containing bulk CoAl-LDHs in conjunction with P25 indicated that the Co:Al ratio had negligible impact on CO_2 photoreduction performance (Figure S2, Supporting Information), and hence the Co:Al stoichiometry was not investigated in this work.

TEM of the parent CoAl-LDH revealed the sand rose structure characteristic of layered double hydroxides, comprising agglomerates of nanoplatelets approximately 40 nm thick (**Figure 1**a,b) and several hundred nanometers across. Successful delamination was directly visualized by TEM, with Figure S1c,d in the Supporting Information and Figure 1c–f evidencing low contrast (as anticipated given their ultrathin nature) sheets in the CoAl-LDH-DS material, with a morphology and diameter similar to those of the parent but whose thickness was decreased from 40 nm to only 2–4 nm (Figure S1c,d, Supporting Information, and Figure 1c,d); the latter dimension is consistent with LDH nanosheets only one to four layers thick as indicated in Figure 1d. Lattice fringes of CoAl-LDH-DS observed in Figure 1f confirmed the delaminated nanosheets were crystalline, with a (d_{012}) spacing of 0.272 nm identical to that of the parent CoAl-LDH.[28] Light scattering upon irradiation of the CoAl-LDH-DS solution by a red laser (the Tyndall effect[30]) evidenced the highly dispersed colloidal nature of the nanosheets, which was stable for >6 months (in contrast the suspended parent CoAl-LDH precipitated within minutes). N_2 porosimetry of both LDH materials (Figure S1b, Supporting Information) showed type II adsorption–desorption isotherms characteristic of macroporous materials (or nonporous materials possessing large interparticle voids) with H3-type hysteresis loops attributed to nonrigid aggregates of plate-like particles under IUPAC classifications.[31] The Brunauer–Emmett–Teller (BET) surface area of CoAl-LDH-DS was 67 m^2 g^{-1}, twice that of the parent CoAl-LDH (36 m^2 g^{-1}).

The morphologies of TiO_2-NT and TiO_2-NP materials were also investigated by XRD and TEM. Figure S3a in the Supporting Information revealed both nanostructured titanias were pure anatase, unlike P25 which is a 4:1 mixture of rutile and anatase phases. **Figure 2** and Figure S4 in the Supporting Information show that the TiO_2-NT comprised uniform, high aspect ratio hollow tubes, with diameters between 6 and 8 nm and

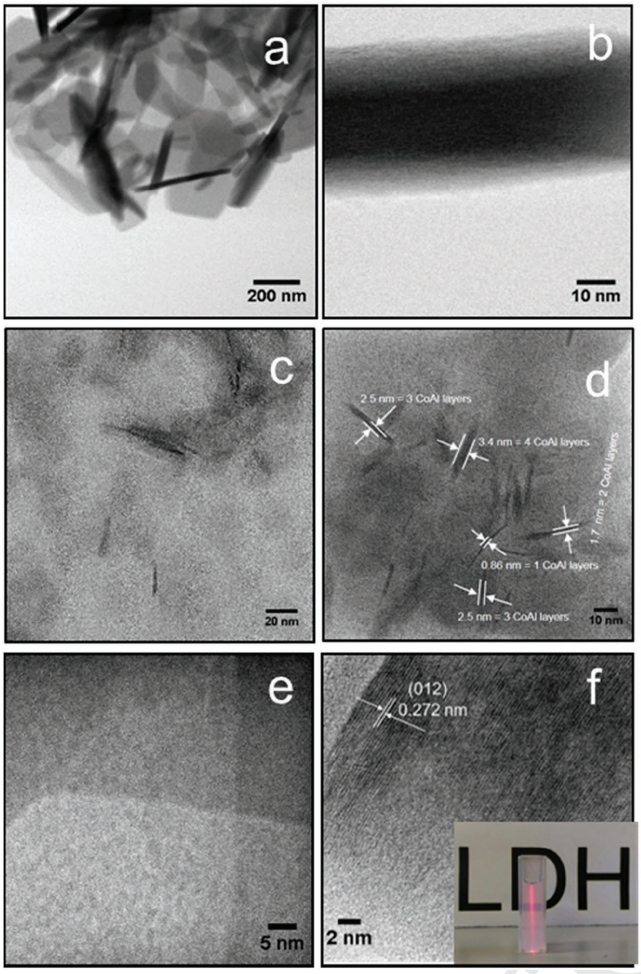

Figure 1. Low and high resolution TEM images of a,b) CoAl-LDH and c–f) CoAl-LDH-DS. Inset photographs show the light scattering behavior of suspended CoAl-LDH particles.

extending for few hundred nanometers in length. The tube wall thickness was <2 nm (Figure S4e,f, Supporting Information), while the (d_{001}) and (d_{101}) planar spacings of 0.24 and 0.35 nm, respectively, confirmed the nanotubes were anatase titania.[32,33] TiO_2-NP comprised uniform, approximately 5 nm diameter spherical anatase particles. These nanostructures were tightly packed in both cases, with the resulting interparticle voids expected to confer micro- or mesoporosity, as reflected in their type IV adsorption-desorption isotherms (Figure S3b, Supporting Information),[31] and high surface areas (229–250 $m^2\ g^{-1}$) relative to nonporous TiO_2-P25 (54 $m^2\ g^{-1}$).

2.2. CoAl-LDH@TiO_2 Nanocomposites

Synthesis of Co-LDH-DS@TiO_2 nanocomposites is summarized in **Scheme 1**. Nanocomposites containing around 3 wt% of the LDH component prepared without a protective N_2 atmosphere suffered partial reconstruction of the delaminated CoAl-LDH-DS, evidenced by a very weak, but characteristic (d_{003}) reflection at 11° by powder XRD (Figure S5, Supporting

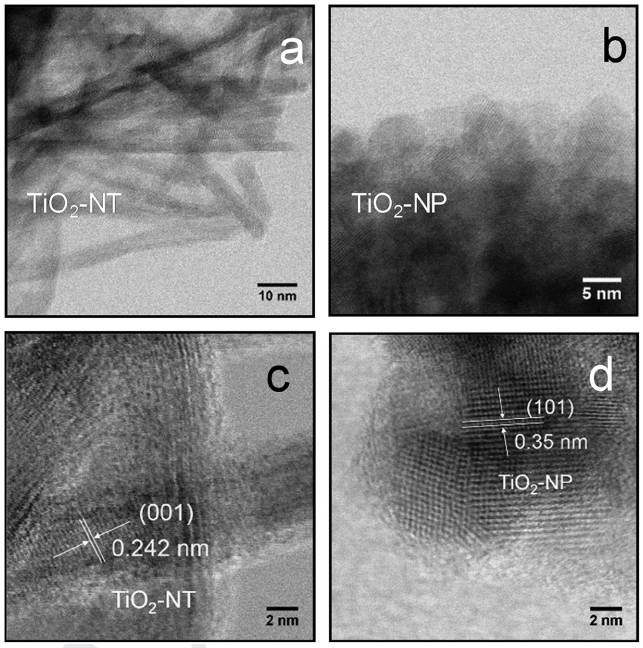

Figure 2. Low and high resolution TEM images of a,c) TiO_2-NT and b,d) TiO_2-NT.

Information), possibly due to the presence of CO_3^{2-} ions from dissolved atmospheric CO_2 attracting LDH sheets together,[29] while those prepared >80 °C resulted in LDH decomposition and concomitant $Al(OH)_3$ and Co_3O_4 (and/or $(Co(OH)_2)$ formation.[34,35] Optimal synthetic conditions were therefore determined as 50 °C under an N_2 atmosphere. A common Co:Al stoichiometry of 2:1 was maintained for all nanocomposites in this work (Table S1, Supporting Information).

High resolution TEM images of 3 wt% LDH-DS@TiO_2-NT and 3 wt% LDH-DS@TiO_2-NP NP (**Figure 3**a,b and Figure S6, Supporting Information) evidence intimate contact between the titania nanostructures and delaminated CoAl-LDH nanosheets, with lattice fringes for each component identical to those observed prior to their mixing. Energy-dispersive X-ray (EDX) elemental mapping confirmed a uniform distribution of CoAl-LDH throughout the titania nanotubes and nanoparticles matrices (Figures S7 and S8, Supporting Information, respectively).

XRD patterns of the preceding nanocomposites exhibited only anatase reflections (Figure S9, Supporting Information, the low CoAl-LDH-DS concentration prohibiting observation of associated reflections) consistent with HRTEM, while a 3 wt% LDH-DS@TiO_2-P25 reference material prepared identically also exhibited anatase and rutile reflections from the parent commercial titania. Volume averaged particles sizes of titania crystallites were unchanged from their parent values (Table S1, Supporting Information). Together with HRTEM, these findings confirm the retention of ordered LDH and titania phases within the nanocomposites. Nitrogen porosimetry of the 3 wt% CoAl-LDH-DS@TiO_2 nanocomposites showed adsorption–desorption isotherms dominated by the parent titania characteristics, with 3–5 nm mesopores evident for the nanotube and nanoparticle materials (Figure S10a,b, Supporting Information),

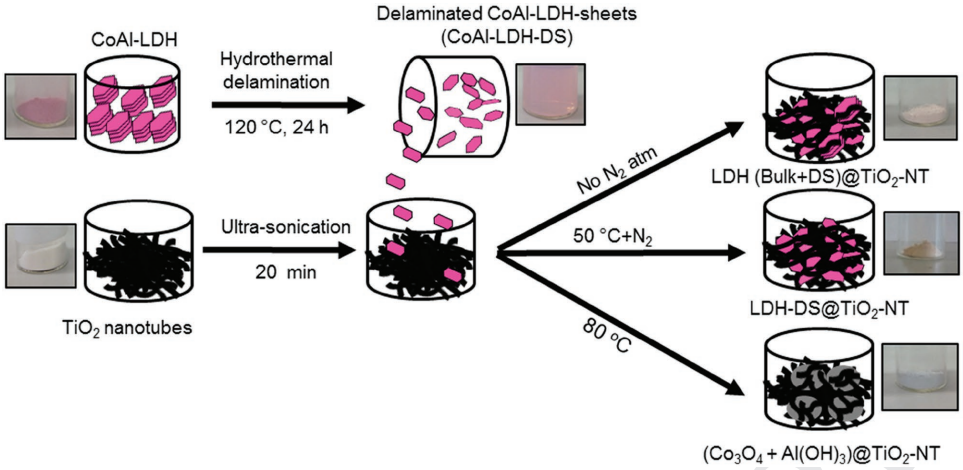

Scheme 1. Schematic of CoAl-LDH@TiO_2 nanocomposite synthesis.

as anticipated from the low loading of LDH incorporated. A slight reduction in surface area (and pore volume and BJH pore diameter) on introducing CoAl-LDH-DS into the nanotube and nanoparticle matrices was observed (Table S1 and Figure S10b, Supporting Information), consistent with that expected for a physical mixture of the two components. HRTEM, XRD, and porosimetry together evidence the successful integration of CoAl-LDH nanosheets only a few layers thick and delaminated along the (d_{00n}) planes within TiO_2 nanostructures.

2.3. Photophysical Properties of CoAl-LDH@TiO_2 Nanocomposites

The electronic structure and optical properties of 3 wt% CoAl-LDH-DS@TiO_2 nanocomposites, and constituent titania and LDH components, were subsequently investigated by XPS, UV–vis and time-resolved photoluminescence (PL) spectroscopies. **Figure 4**a shows Ti 2p XP spectra for the parent titania nanotubes and nanoparticles, alongside their corresponding nanocomposites. In all cases, a single spin–orbit split doublet was observed with $2p_{3/2}$ and $2p_{1/2}$ peaks centered around 458.1 and 463.7 eV, respectively, consistent with Ti^{4+} species in TiO_2.[28] The Co 2p XP spectrum of CoAl-LDH-DS also exhibited a single spin–orbit split doublet (Figure 4b) and hence chemical environment, with $2p_{1/2}$ and $2p_{3/2}$ peaks centered around 796.7 and 780.8 eV and satellites at 801.3 and 786.5 eV indicative of high-spin divalent Co^{2+} species within the CoAl-LDH layers.[36] A small increase in the Co $2p_{3/2}$ binding energy (to 781.3 eV), and concomitant decrease in the Ti $2p_{3/2}$ binding energy (to 457.8 eV), was observed for the 3 wt% CoAl-LDH-DS@TiO_2-NT relative to the individual components. This may reflect an initial state effect arising from electron transfer from the CoAl-LDH-DS to TiO_2-NT component and provides tentative evidence for direct electronic contact (heterojunction formation) between the semiconductors.

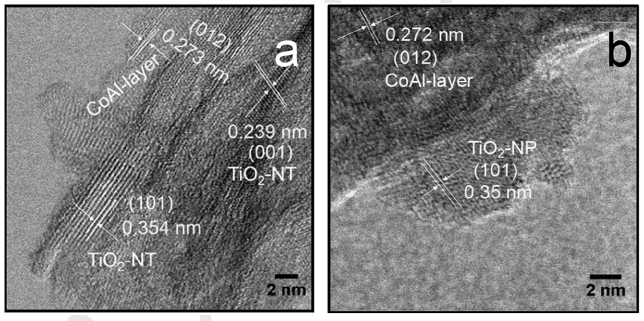

Figure 3. High resolution TEM images a) 3 wt% LDH-DS@TiO_2-NT and b) LDH-DS@TiO_2-NP nanocomposites.

Diffuse reflectance UV–vis (DRUV) spectra of 3 wt% CoAl-LDH-DS@TiO_2 nanocomposites, and constituent titania and LDH components are shown in Figure 4c. All titania materials exhibited strong UV absorption, with a sharp cutoff ≈380 nm for nanotubes and ≈390 nm for anatase nanoparticles and P25, translating to optical band gaps of 3.21 (TiO_2-NT) and 3.14 eV (TiO_2-NP) (Figure S11a,b, Supporting Information).[37] The slight band gap widening for the TiO_2-NT may arise from quantum confinement effects[38] within the thin (<2nm) walls, which are expected as the semiconductor dimensions fall below twice the exciton Bohr radius (estimated between 1 and 3.2 nm for anatase[39,40]). The DRUV spectrum of CoAl-LDH exhibited two distinct absorption bands, a broad band in the visible region centered around 558 nm, and a sharper UV band around 300 nm; delamination shifted the middle band to ≈520 nm, and resulted in the appearance of additional absorption band around 670 nm. The bands 520–558 nm are indicative of the 4T1g(F) →4T1g(P) transition of Co^{2+} octahedrally coordinated by weak-field ligands,[27,41] while that at 670 nm band corresponds to a 3A2g(F)→3T1g(F) transition arising from spin–orbit coupling.[41,42] The UV absorption may arise from ligand → metal charge transfer within the CoAl-LDH layer. These absorption features translate to optical band gaps of 2.12 and 2.18 eV for CoAl-LDH and CoAl-LDH-DS, respectively (Figure S11c,d, Supporting Information), consistent with literature reports.[28,43] The 3 wt% CoAl-LDH@TiO_2 nanocomposites exhibited spectra intermediate between those of their constituent components, albeit dominated by the majority titania component, featuring strong UV absorption arising from TiO_2 nanotubes/nanoparticles and a weak visible light response from the delaminated

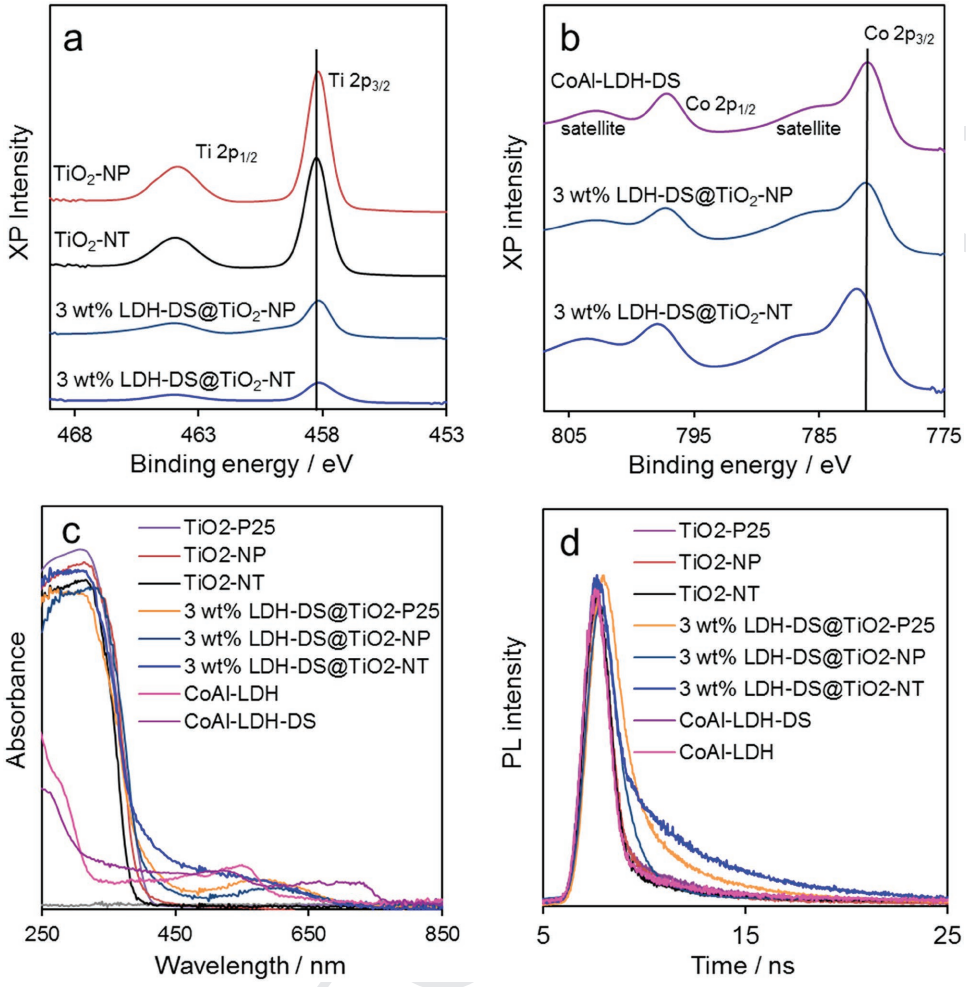

Figure 4. a) Ti 2p and b) Co 2p XP spectra, c) DRUVS, and d) time-resolved PL spectra at 380 nm excitation wavelength of 3 wt% LDH-DS@TiO_2 nanocomposites alongside CoAl-LDH and TiO_2 references.

CoAl-LDH nanosheets. Heterojunction formation between semiconductor components is indicated by a shift in the nanocomposite UV absorption cutoffs to higher wavelength relative to the pure TiO_2 nanostructures, particularly noticeable for the 3 wt% CoAl-LDH@TiO_2-NT material.

VBM edge potentials of titania and CoAl-LDH-DS components were also determined by valence band XPS[27] (Figure S12, Supporting Information) from the intercept of the tangent to the density of states at the Fermi edge as 2.69 eV (TiO_2-NP), 2.75 eV (TiO_2-NT), and 1.25 eV (CoAl-LDH-DS). These VBM were used in conjunction with the preceding optical band gap energies to calculate corresponding conduction band minimum (CBM) potentials of −0.45 eV (TiO_2-NP), −0.46 eV (TiO_2-NT), and −0.93 eV (CoAl-LDH-DS).[25] These energy levels and associated band offsets are shown in Figure S13 in the Supporting Information, and indicative of a type-II (staggered) band alignment at the CoAl-LDH-DS@TiO_2 interface, with ΔE_{VBM} = 0.42 eV and 1.29 eV and ΔE_{CBM} = 0.26 eV and 0.27 eV for the 3 wt% CoAl-LDH-DS@TiO_2-NT and 3 wt% CoAl-LDH-DS@TiO_2-NP, respectively. Heterojunction formation is accompanied by band bending between the CoAl-LDH-DS and TiO_2 components. This band alignment is considered advantageous for the separation of photogenerated holes and electrons,[44] favoring hole accumulation on the CoAl-LDH-DS nanosheets (and consequent water oxidation) and electron accumulation on the titania nanostructures (and consequent CO_2 reduction), and hence both halves of the full redox reaction without additional (molecular) charge acceptors.

Photoinduced charge carrier recombination within the 3 wt% CoAl-LDH-DS@TiO_2 nanocomposites, and Co-Al-LDH-DS and TiO_2 reference materials, was probed through steady state[45] and time-resolved[46] PL spectroscopy. All TiO_2 nanostructures exhibited two characteristic emissions under irradiation with 320 nm light (Figure S14, Supporting Information); one around 400 nm arising from an interband transition[47] and a second weaker emission around 470 nm attributed to the recombination of charges localized on oxygen vacancies.[47] CoAl-LDH and CoAl-LDH-DS also exhibited two emissions at 400 and 470 nm, attributed to ligand field splitting and corresponding 4A2g → 4T1g (F) and 4T2g → 4T1g (F) transitions often reported for octahedral cobalt(II) compounds.[46,41] The emissions in CoAl-LDH-DS were significantly reduced relative to the parent CoAl-LDH, indicating suppressed charge recombination. Despite the high titania loading in all three 3 wt% CoAl-LDH-DS@TiO_2

nanocomposites, their corresponding emissions were significantly reduced relative to the parent TiO_2 component, indicating suppressed charge recombination (improved charge separation), presumably due to the migration of photoexcited electrons from the CB of CoAl-LDH-DS to that of the TiO_2 matrix, and concomitant photoexcited hole migration from the VB of the TiO_2 matrix to the VB of CoAl-LDH-DS. Emission from the 3 wt% CoAl-LDH-DS@TiO_2-NT was especially weak compared to its nanoparticle and P25 analogues, possibly due to more extensive heterojunction formation observed by XPS and greater valence band bending (ΔE_{VBM} decreasing from 1.5 → 0.42 for the nanotube composite vs 1.44 → 1.29 for the nanoparticle analogue).

Time-resolved PL measurements provided additional confirmation for reduced charge carrier recombination within the 3 wt% LDH-DS@TiO_2 nanocomposites (Figure 4d).[46] Average charge carrier lifetimes (τ) were determined from fitting the resulting decay curves with a biexponential function (Table S2, Supporting Information), which reflect nonradiative and radiative relaxation processes originating from the direct formation of free charge carriers and the indirect formation of self-trapped excitons. In all cases, the nanocomposites displayed longer τ values (i.e., slower recombination) than their CoAl-LDH-DS and TiO_2 constituents, with the 3 wt% CoAl-LDH-DS@TiO_2-NT exhibiting the slowest electron–hole pair recombination of τ = 6.7 ns versus 5.5 ns (TiO_2-NT) and 4.8 ns (CoAl-LDH-DS). This modified electronic transport provides further evidence for heterojunction formation (and an excellent synergy) between the delaminated CoAl-LDH nanosheets and the TiO_2 matrices they are dispersed within.

2.4. Photocatalytic CO_2 Reduction over CoAl-LDH@TiO_2 Nanocomposites

The photocatalytic performance of CoAl-LDH@TiO_2 nanocomposites was subsequently investigated for aqueous phase CO_2 reduction under UV–vis irradiation by a 300 W Xe lamp in the absence of a sacrificial hole acceptor. Control experiments were first performed in the absence of either CO_2, water, catalyst, or light (Figure S15, Supporting Information) to confirm that CO_2 and water were the only sources of carbon and hydrogen in photocatalytic products.[27,48] Only gaseous products of photocatalysis were observed, namely CO_2, H_2, O_2, and (exceptionally) methane.

Individual TiO_2 nanostructures (P25, TiO_2-NP, and TiO_2-NT) exhibited very low activity for either CO_2 reduction or water oxidation (**Figure 5** and Table S3, Supporting Information), presumably due to a combination of their small CBM potentials (≈–0.45 eV) which is insufficient to drive effectively $CO_2 + 2H + 2e^- \rightarrow CO + H_2O$ (E^0 = –0.53 eV at pH 7), fast photoexcited charge carrier recombination and low CO_2 absorptivity (Table S1, Supporting Information). However, this CBM potential is sufficient to drive proton reduction to hydrogen (–0.41 eV at pH 7), and indeed H_2 was evolved over all titanias, albeit at a low rate due to rapid charge recombination commonly observed in the absence of either a noble metal cocatalyst to trap photo-excited electrons, and/or organic scavengers to trap photoexcited holes.[14] Among the titanias, TiO_2-NTs exhibited the highest photocatalytic activity, which we attribute to its high aspect ratio, thin walls, comparatively slow charge recombination (τ = 5.5 ns vs 4.8 and 1.5 ns for TiO_2-NP and P25, respectively) and short diffusion length for photoexcited charges to reach the nanotube surface. The parent Co-Al-LDH and delaminated CoAl-LDH-DS nanosheets both exhibited slightly improved CO production relative to titanias (as expected for their higher CBM potential of ≈–0.93 eV), with delamination conferring a 20% enhancement (1.06 vs 0.83 μmol h^{-1} g^{-1}) as a result of the associated increase in surface area and CO_2 adsorption capacity seen in Table S1 in the Supporting Information, and concomitant decrease in charge recombination shown in Figure 4d and Table S2 in the Supporting Information. However, neither performance was especially impressive, likely an inability to drive both sides of the redox reaction in the absence of a charge carrier acceptor. In contrast, all CoAl-LDH@TiO_2 nanocomposites showed superior CO productivity to and hence a strong synergy between the LDH and titania components. The 3 wt% CoAl-LDH-DS@TiO_2-NT nanocomposite exhibited the highest CO productivity of 4.57 μmol g^{-1} h^{-1}, almost 7.5 and 5 times that of its TiO_2-NT and CoAl-LDH-DS constituents, respectively (and twice that of 20 wt% P25@CoAl-LDH),[27] in addition to 0.41 μmol g^{-1} h^{-1} CH_4; this equates to a CO+CH_4 selectivity >94% (Table S3, Supporting Information). This synergy must arise from a convolution of increased spectral utilization (UV and visible), charge carrier separation/lifetime, and CO_2 affinity for the heterojunction nanocomposite. All components and nanocomposites displayed (CO or H_2):O_2 product stoichiometries close to 2:1, as expected since CO_2 reduction to CO and H_2O reduction to H_2 are both $2e^-$ processes, whereas water oxidation is a $4e^-$ process ($2H_2O \rightarrow O_2 + 4H^+ + 4e^-$). For 3 wt% CoAl-LDH-DS@TiO_2-NT, a CH_4:O_2 stoichiometry of 1:2 was also observed, consistent with the $8e^-$ reduction to form methane from CO_2. It is noteworthy that methane was only produced over the 3 wt% LDH-DS@TiO_2-NT photocatalyst, which exhibits the longest charge carrier lifetimes (Table S2, Supporting Information), consistent with the slower kinetics expected for this more demanding multielectron reduction.

CO productivity over the 3 wt% CoAl-LDH-DS@TiO_2-NT photocatalyst was more than double that achieved for the 3 wt% CoAl-LDH@TiO_2-NT or 3 wt% LDH-DS@TiO_2-NP materials. The physicochemical properties including phase, crystallite size, surface area, and CO_2 chemisorption capacity of these three photocatalysts are almost identical (Table S1, Supporting Information), as are the optical band gaps of their CoAl-LDH/CoAl-LDH-DS and TiO_2-NT/TiO_2-NP components. Hence, this rate enhancement can only be ascribed to more efficient heterojunction formation between visible light absorbing delaminated CoAl-LDH-DS nanosheets and UV light absorbing high aspect ratio TiO_2 nanotubes in the 3 wt% CoAl-LDH-DS@TiO_2-NT.

The impact of heterojunction formation and role of the titania component in the nanocomposites was further examined by comparing UV–vis versus visible light (employing a 400 nm cutoff filter) photocatalytic CO_2 reduction over the 3 wt% LDH-DS@TiO_2-NT and constituent TiO_2 nanotube and CoAl-LDH-DS. Under visible light irradiation, the nanotubes were catalytically inactive, as expected for the wide band gap semiconductor, whereas the CoAl-LDH-DS evolved small quantities of CO and O_2 (**Figure 6**). However, the lower CO and CH_4

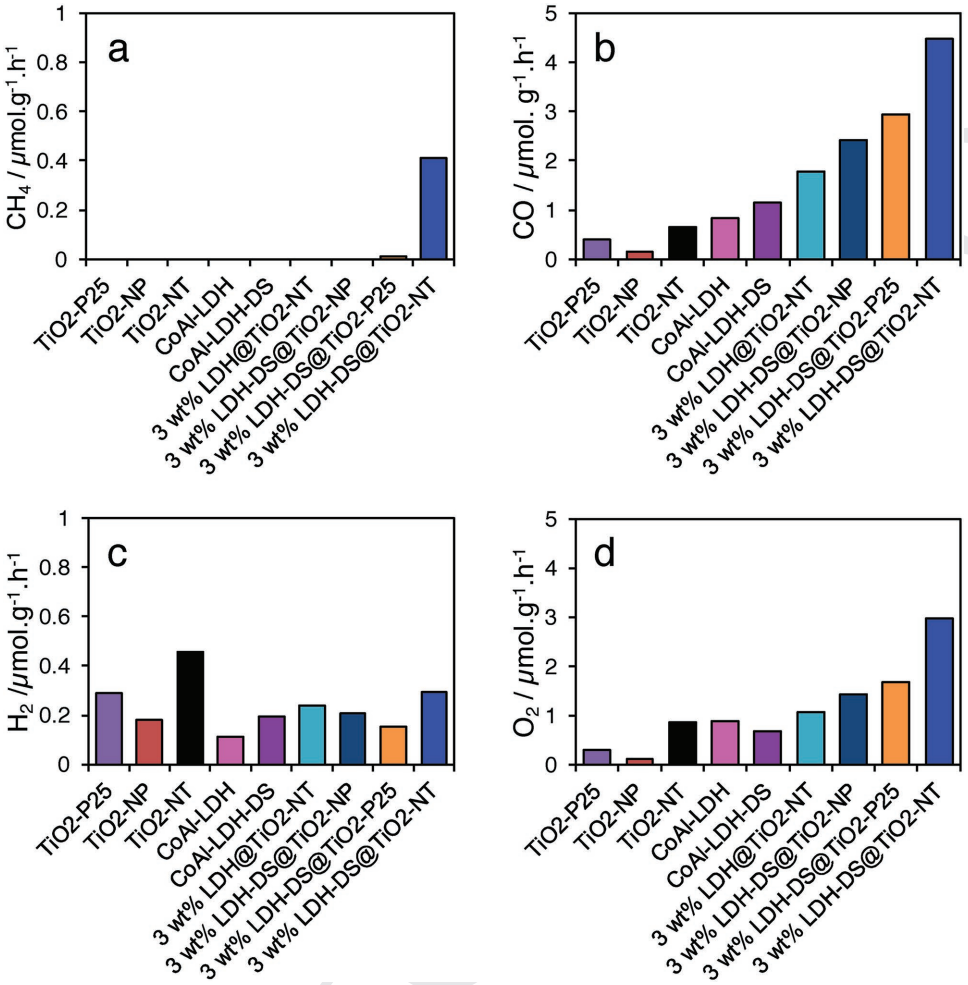

Figure 5. a) CH_4, b) CO, c) H_2, and d) O_2 mass-normalized productivity averaged over the first 4 h of aqueous phase CO_2 photoreduction over 3 wt% LDH-DS@TiO_2 nanocomposites, and CoAl-LDH and TiO_2 references under UV–vis irradiation by a 300 W Xe lamp.

reduction productivities of the nanocomposite compared to those observed under UV–vis irradiation (2.0 vs 4.5 μmol h^{-1} g^{-1} CO and 0.1 vs 0.4 μmol h^{-1} g^{-1} CH_4) suggest that significant electron–hole recombination occurs within the delaminated CoAl-LDH-DS nanosheets in the absence of simultaneous titania photoexcitation, i.e., two-step photon excitation of both semiconductors is superior to LDH excitation alone. Under UV–vis irradiation, titania can act as both a hole-donor, promoting water oxidation over the LDH, and as an electron-acceptor. This observation highlights the importance of change separation across the heterojunction interface of 3 wt% LDH-DS@TiO_2-NT nanocomposite in enhancing the poor intrinsic visible light photo-oxidation activity of the delaminated CoAl-LDH-DS and poor intrinsic UV photoreduction activity of TiO_2-NT. Apparent quantum efficiencies (AQE) for CO production over 3 wt% LDH-DS@TiO_2-NT are around 0.26% and 0.09% under 365 nm (using a UV band pass filter) and 475 nm (visible band pass filter) irradiation (Table S4, Supporting Information), respectively. These AQEs are much higher than corresponding values of <0.1% (UV) for P25@CoAl-LDH[27] or reduced graphene oxide-amine-titanium dioxide nanocomposites[49] or $ZrOCo^{II}$–IrO_x SBA-15[50] wafer or Pt-TiO_2[51] heterogeneous photocatalysts. They are also much greater than many "high performance" photocatalysts such as TiO_2 nanofibers (0.036%)[52] and $SrNb_2O_6$ plates (0.065%)[51] under UV irradiation, and Co_3O_4 hexagonal platelets under visible light[53] (0.069%, wherein a visible light sensitizer $[Ru(bpy)_3]Cl_2$ and hole scavenger TEOA were also required). The combined quantum efficiency for CO+CH_4 is also higher than those reported Ag/Ag_2SO_3 (0.12%)[54] and $Ag/AgIO_3$ (0.19%),[55] photocatalysts for CO_2 reduction to CO+CH_4, featuring noble metal electron traps and water vapor as the proton donor (albeit CH_4 was the major product).

Photocatalytic CO_2 reduction over 3 wt% CoAl-LDH-DS@TiO_2-NT is proposed to occur in a similar fashion to that previously advanced.[27] Briefly, under visible light irradiation, due to the type-II band alignment between the LDH and titania, electrons photoexcited into the LDH conduction band migrate via the heterojunction into the titania conduction band, where they reduce CO_2 (adsorbed at the LDH surface) into CO and CH_4 as illustrated in **Scheme 2**. Under UV irradiation, photoexcited holes simultaneously migrate from valence band of titania via the heterojunction into the LDH valence band, where they may be trapped at Co^{2+} sites to produce Co^{3+} or Co^{4+} which in turn

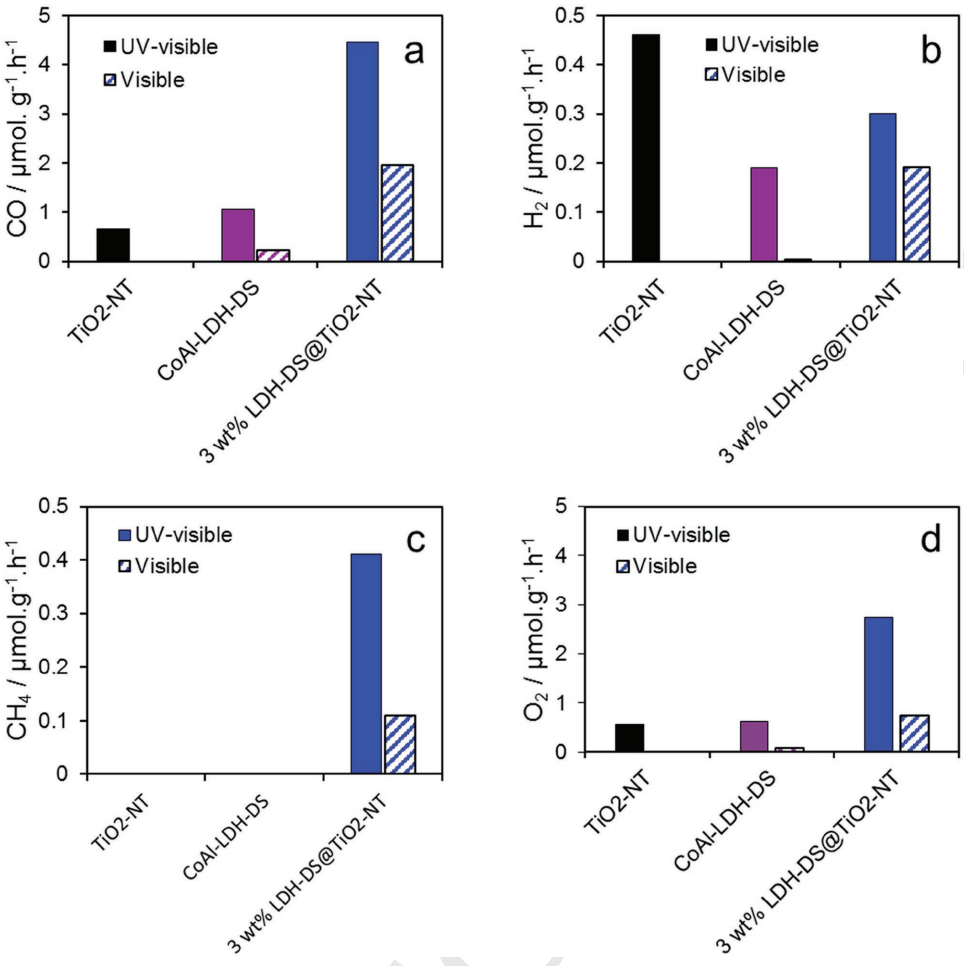

Figure 6. Comparison of a) CH_4, b) CO, c) H_2, and d) O_2 mass-normalized productivity averaged over the first 4 h of aqueous phase CO_2 photoreduction over 3 wt% LDH-DS@TiO_2-NT nanocomposite, and CoAl-LDH-DS and TiO_2-NT references under UV–vis versus visible only light irradiation.

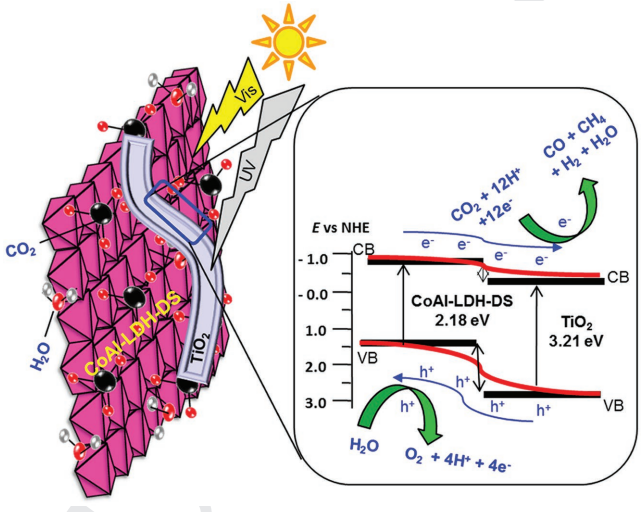

Scheme 2. Proposed mechanism of CO_2 photocatalytic reduction over CoAl-LDH-DS@TiO_2-NT heterojunction nanocomposite.

oxidize H_2O to liberate O_2, regenerate Co^{2+}, and release protons which migrate to the interface with titania where they combine with electrons and/or molecular carbon species to form H_2, CO, or CH_4.[56,57] The combination of delaminated CoAl-LDH-DS nanosheets and high aspect ratio anatase TiO_2 nanotubes creates a large heterojunction interface across which photoinduced charge carrier separation, and the preceding redox chemistry, can occur. Such charge separation extends charge carrier lifetimes sufficient to facilitate the challenging multielectron reduction of CO_2 to CH_4. Delaminated CoAl-LDH-DS nanosheets promote aqueous phase catalytic CO_2 photoreduction by harnessing visible light, adsorbing CO_2 from solution, and promoting water oxidation. Future studies will explore routes to induce ordering between the LDH and anatase components, for example, through surfactant templating approaches and/or spatial localization within hierarchically porous scaffolds,[59] and to further improve the heterojunction interface through either reducing the dimensions of the delaminated CoAl-LDH nanosheets, or shortening the anatase nanotubes to enhance interpenetration between the semiconductor components.

3. Conclusion

A facile wet-chemical route has been developed to prepare CoAl-LDH-DS@TiO_2 nanocomposites via the dispersion of (visible light absorbing) delaminated CoAl-layered double hydroxide nanosheets within matrices of (UV absorbing) anatase NT or NP. The resulting CoAl-LDH-DS@TiO_2 nanocomposites show significant rate enhancements and improved apparent quantum efficiency for the aqueous phase catalytic CO_2 photoreduction to CO and CH_4, in the absence of sacrificial agents. Maximum CO productivity was obtained for 3 wt% CoAl-LDH@TiO_2-NT, being 5–7.5 times higher than that of its constituent TiO_2 or delaminated CoAl-LDH nanosheet components, and more than twice as active as nanocomposites containing either bulk CoAl-LDH or anatase NPs. Superior photocatalytic reduction of the CoAl-LDH-DS@TiO_2 nanocomposites reflects formation of a staggered type-II heterojunction across the interface between these high aspect ratio semiconductors, which permits efficient photoexcited charge separation resulting from electron transfer from the CoAl-LDH-DS to titania, and concomitant reverse hole transfer from titania into the CoAl-LDH TiO_2 nanostructure. Selectivity to ($CO + CH_4$) reached >90% relative to H_2 evolution under full spectrum irradiation. This synthetic strategy could be readily extended to prepare diverse mixed oxide/hydroxide nanocomposites for applications including water splitting, waste water depollution, fuel cells, and energy storage.

4. Experimental Section

Materials: Reagents $Co(NO_3)_2{\cdot}6H_2O$ (Sigma, 99%), $Al(NO_3)_3{\cdot}9H_2O$ (Sigma, 99%), P25 (Sigma), and hexamine (Sigma, 99.9%), titanium (IV) *n*-butoxide (ACROS Organics, 99.0%), sulfuric acid (Fisher, 98%), hydrochloric acid (Fisher, 37%), ethanol (Fisher, analytical reagent grade), sodium hydroxide (ACROS Organics, 99%) were used as received. All other chemical reagents used in this work were analytical grade and used without further purification.

TiO_2 Nanostructures Synthesis: TiO_2 nanoparticles and nanotubes were synthesized following solvothermal and hydrothermal literature methods (Scheme S1a, Supporting Information).[58] For anatase TiO_2 nanoparticles (TiO_2-NP), 5.1 g titanium (IV) *n*-butoxide was added dropwise to 70 mL absolute ethanol under vigorous stirring at room temperature, followed by 0.33 mL sulfuric acid and 0.3 mL deionized water. The resulting solution was transferred to a 100 mL Teflon autoclave and aged for 4 h at 180 °C under air to yield a white solid, which was then washed thoroughly with ethanol and dried at 60 °C for 5 h. For anatase TiO_2 nanotubes (TiO_2-NT), 0.5 g of the preceding TiO_2-NP was added to a 50 mL 10 M NaOH aqueous solution in a Teflon autoclave at room temperature, and aged for 24 h at 150 °C for 24 h. The resulting solid was dispersed in 500 mL 0.1 M HCl aqueous solution for 12 h under constant stirring at room temperature, then centrifuged (5000 rpm and 5 min) and washed thoroughly with deionized water and subsequently ethanol, dried at 60 °C for 5 h, and finally calcined at 400 °C for 2 h under flowing O_2 (20 mL min^{-1}).

LDH Nanostructure Synthesis: CoAl-LDH (Scheme S1b, Supporting Information) and delaminated CoAl-LDH nanosheets were prepared following a (carbonate-free) hydrothermal literature method.[29] For the parent CoAl-LDH, 0.06 mols $Co(NO_3)_2{\cdot}6H_2O$, 0.03 mols $Al(NO_3)_3{\cdot}9H_2O$, and 0.012 mols hexamethylenetetramine were dissolved in 200 mL deionized and degassed water. The resulting solution was purged with N_2 at room temperature under constant stirring, and then aged in a 500 mL round bottom flask at 80 °C for 48 h under N_2 without stirring. The precipitate (cake) obtained was washed with deionized water until the washing were of neutral pH, and subsequently dried overnight at 60 °C in vacuo to yield the final CoAl-LDH which was stored in a vacuum desiccator. Delaminated CoAl-LDH nanosheets (LDH-DS) were prepared by adding 2.5 g of the preceding pH neutral CoAl-LDH cake to 50 mL deionized and degassed water in a Teflon autoclave, prior to ageing at 120 °C for 12 h. Residual parent CoAl-LDH was removed by centrifugation at 2000 rpm for 30 min, leaving a colloidal solution of the CoAl-LDH-DS material (2.4 g L^{-1}) which was purged with N_2 at 50 °C, sealed with parafilm and stored in a desiccator. A powder reference sample of delaminated CoAl-LDH nanosheets was also prepared by evaporation of the colloidal solution under N_2.

CoAl-LDH@TiO_2 Nanocomposites Synthesis: CoAl-LDH@TiO_2 nanocomposites were prepared by ultrasonic dispersion followed by deposition-evaporation. Briefly, 200 mg of synthesized TiO_2-NT, TiO_2-NP, or commercial TiO_2-P25 was dispersed in deionized and degassed water by ultrasonication (Elmasonic S100H, 5 min, 550 W/50 Hz), to which a desired mass of parent CoAl-LDH, or volume of CoAl-LDH-DS colloidal solution, was added. The resulting suspension was stirred at room temperature under N_2 for 24 h, and water subsequently evaporated at 50 °C to yield the nanocomposite. The mass of CoAl-LDH-DS was also varied from 1 to 5 wt% to produce a family of CoAl-LDH-DS@TiO_2-NT composites. Note that composites containing 3 wt% CoAl-LDH-DS were the most active for the photocatalytic reduction of CO_2 (Figure S16, Supporting Information) and hence were selected for detailed study in this work.

Catalyst Characterization: Powder XRD patterns were recorded on a Bruker-AXS D8 ADVANCE diffractometer operated at 40 kV and 40 mA using Cu K_α radiation (0.15418 nm) between 10° and 80° in 0.02° steps. X-ray photoelectron spectroscopy was performed on a Kratos Axis HSi spectrometer with a monochromated Al K_α X-ray source operated at 90 W and magnetic charge neutralizer. Spectral processing was performed using CasaXPS version 2.3.16, with energy referencing to adventitious carbon at 284.6 eV, and surface compositions and peak fitting derived using appropriate instrumental response factors and common line shapes for each element. Nanostructure morphology was visualized on a JEOL JEM-2100 HAADF-STEM operating at 200 kV accelerating voltage, with elemental mapping performed by EDX spectroscopy using an Oxford INCA EDX detector. Porosimetry was performed through N_2 physisorption at 77 K using a Quantachrome Nova 4000e porosimeter. BET surface areas were calculated over the relative pressure range 0.01–0.2. Pore size distributions were calculated by applying the BJH method to desorption isotherms for relative pressures >0.35. CO_2 chemisorption was performed on samples degassed at 120 °C using an He carrier gas on a Quantachrome ChemBET PULSAR TPR/TPD/TPO instrument. Diffuse reflectance UV–vis spectra (DRUVS) were measured on a Thermo Scientific Evo220 spectrometer using an integrating sphere and KBr as standard and samples diluted in KBr. Optical band gaps were calculated from Tauc plots as described in the Supporting Information. Steady state PL spectra of samples were recorded on an F-4500FL spectrometer at an excitation wavelength of 320 nm. PL lifetime data were collected on an Edinburgh Photonics FLS 980 spectrometer using a picosecond pulsed LED light with an excitation wavelength of 380 nm.

Photocatalytic CO_2 Reduction: Photocatalytic CO_2 reduction was carried out at room temperature in a sealed 320 mL stainless steel photoreactor with a quartz window and a 300 W Xe light source. 50 mg of sample was dispersed in 5 mL of water by ultrasonication for 5 min and charged in the photoreactor. Prior to irradiation, the reaction mixture was degassed in the dark with CO_2 at 1 bar for 2 h to saturate the solution with CO_2 and then continuously irradiated with UV–vis light using a 300 W Xe Toption Group Ltd TOP-X300 lamp (spectral output shown in our previous report[27]). Aliquots of the reaction mixture were periodically withdrawn using a 1 mL gas syringe for analysis on a Shimadzu Tracera GC-2010 Plus chromatograph fitted with a Carboxen1010 (30 m × 0.53 mm × 0.1 µm) column and Barrier Ionization Detector. Liquid products were also analyzed periodically from separate aliquots on an Agilent 1260 HPLC fitted with a Hi Plex column; no carbon-containing liquid products were detected in this study. P25 was calcined in air at 200 °C for 4 h prior to use in control experiments to remove any trace carbonaceous residues; without calcination, small quantities of CO and

CH_4 were evolved during control experiments under nitrogen in the absence of CO_2. Selectivity toward reactively formed H_2, CO, and CH_4 was calculated from Equations (1)–(3)[27]

$$H_2\ \text{selectivity}(\%) = \frac{2N_{H_2}}{8N_{CH_4} + 2N_{CO} + 2N_{H_2}} \times 100 \quad (1)$$

$$CO\ \text{selectivity}(\%) = \frac{2N_{CO}}{8N_{CH_4} + 2N_{CO} + 2N_{H_2}} \times 100 \quad (2)$$

$$CH_4\ \text{selectivity}(\%) = \frac{2N_{CH_4}}{8N_{CH_4} + 2N_{CO} + 2N_{H_2}} \times 100 \quad (3)$$

where N_{CH_4}, N_{CO}, and N_{H_2} are the yields of reactively formed CH_4, CO, and H_2, respectively. Apparent quantum yields were calculated as described in the Supporting Information at either 365 (UV) or 475 (Visible) nm.

Supporting Information

Supporting Information is available from the Wiley Online Library or from the author.

Acknowledgements

The authors thank the EPSRC (EP/K021796/1 and EP/K029525/2) for financial support.

Conflict of Interest

The authors declare no conflict of interest.

Keywords

CO_2, layered double hydroxides, nanocomposites, photocatalysis, titania

Received: August 30, 2017
Revised: September 27, 2017
Published online:

[1] T. Faunce, S. Styring, M. R. Wasielewski, G. W. Brudvig, A. W. Rutherford, J. Messinger, A. F. Lee, C. L. Hill, H. deGroot, M. Fontecave, D. R. MacFarlane, B. Hankamer, D. G. Nocera, D. M. Tiede, H. Dau, W. Hillier, L. Wang, R. Amal, *Energy Environ. Sci.* **2013**, *6*, 1074.
[2] P. V. Kamat, *J. Phys. Chem. C* **2007**, *111*, 2834.
[3] W. Tu, Y. Zhou, Z. Zou, *Adv. Mater.* **2014**, *26*, 4607.
[4] D. Chen, X. Zhang, A. F. Lee, *J. Mater. Chem. A* **2015**, *3*, 14487.
[5] L. Zhang, Z.-J. Zhao, J. Gong, *Angew. Chem., Int. Ed.* https://doi.org/10.1002/anie.201612214.
[6] K. Nakata, A. Fujishima, *J. Photochem. Photobiol., C* **2012**, *13*, 169.
[7] J. L. Gole, J. D. Stout, C. Burda, Y. Lou, X. Chen, *J. Phys. Chem. B* **2004**, *108*, 1230.
[8] Y. Ma, X. Wang, Y. Jia, X. Chen, H. Han, C. Li, *Chem. Rev.* **2014**, *114*, 9987.
[9] M. Ni, M. K. H. Leung, D. Y. C. Leung, K. Sumathy, *Renewable Sustainable Energy Rev.* **2007**, *11*, 401.
[10] S. N. Habisreutinger, L. Schmidt-Mende, J. K. Stolarczyk, *Angew. Chem., Int. Ed.* **2013**, *52*, 7372.
[11] A. T. Garcia-Esparza, K. Takanabe, *J. Mater. Chem. A* **2016**, *4*, 2894.
[12] J. H. Montoya, L. C. Seitz, P. Chakthranont, A. Vojvodic, T. F. Jaramillo, J. K. Norskov, *Nat. Mater.* **2017**, *16*, 70.
[13] R. Abe, K. Sayama, H. Sugihara, *J. Phys. Chem. B* **2005**, *109*, 16052.
[14] A. Kudo, Y. Miseki, *Chem. Soc. Rev.* **2009**, *38*, 253.
[15] N. S. Lewis, *Science* **2007**, *315*, 798.
[16] H. Zhou, R. Yan, D. Zhang, T. Fan, *Chem. – Eur. J.* **2016**, *22*, 9870.
[17] K. Teramura, S. Iguchi, Y. Mizuno, T. Shishido, T. Tanaka, *Angew. Chem., Int. Ed.* **2012**, *51*, 8008.
[18] N. Ahmed, Y. Shibata, T. Taniguchi, Y. Izumi, *J. Catal.* **2011**, *279*, 123.
[19] Y. Zhao, X. Jia, G. I. N. Waterhouse, L.-Z. Wu, C.-H. Tung, D. O'Hare, T. Zhang, *Adv. Energy Mater.* **2016**, *6*, 1501974.
[20] Y. Zhao, G. Chen, T. Bian, C. Zhou, G. I. N. Waterhouse, L.-Z. Wu, C.-H. Tung, L. J. Smith, D. O'Hare, T. Zhang, *Adv. Mater.* **2015**, *27*, 7824.
[21] K.-I. Katsumata, K. Sakai, K. Ikeda, G. Carja, N. Matsushita, K. Okada, *Mater. Lett.* **2013**, *107*, 138.
[22] J. Hong, W. Zhang, Y. Wang, T. Zhou, R. Xu, *ChemCatChem* **2014**, *6*, 2315.
[23] S. Liu, N. Zhang, Z.-R. Tang, Y.-J. Xu, *ACS Appl. Mater. Interfaces* **2012**, *4*, 6378.
[24] S.-M. Xu, H. Yan, M. Wei, *J. Phys. Chem. C* **2017**, *121*, 2683.
[25] S.-M. Xu, T. Pan, Y.-B. Dou, H. Yan, S.-T. Zhang, F.-Y. Ning, W.-Y. Shi, M. Wei, *J. Phys. Chem. C* **2015**, *119*, 18823.
[26] Y. Surendranath, D. G. Nocera, in *Progress in Inorganic Chemistry*, John Wiley & Sons, Inc., **2011**, p. 505.
[27] S. Kumar, M. A. Isaacs, R. Trofimovaite, L. Durndell, C. M. A. Parlett, R. E. Douthwaite, B. Coulson, M. C. R. Cockett, K. Wilson, A. F. Lee, *Appl. Catal., B* **2017**, *209*, 394.
[28] Y. Dou, S. Zhang, T. Pan, S. Xu, A. Zhou, M. Pu, H. Yan, J. Han, M. Wei, D. G. Evans, X. Duan, *Adv. Funct. Mater.* **2015**, *25*, 2243.
[29] C. A. Antonyraj, P. Koilraj, S. Kannan, *Chem. Commun.* **2010**, *46*, 1902.
[30] F. Song, X. Hu, *Nat. Commun.* **2014**, *5*, 4477.
[31] K. S. W. Sing, D. H. Everett, R. A. W. Haul, L. Moscou, R. A. Pierotti, J. Rouquerol, T. Siemieniewska, in *Handbook of Heterogeneous Catalysis*, Wiley-VCH Verlag GmbH & Co. KGaA, **2008**.
[32] X. Zheng, D. Yu, F.-Q. Xiong, M. Li, Z. Yang, J. Zhu, W.-H. Zhang, C. Li, *Chem. Commun.* **2014**, *50*, 4364.
[33] J. Ding, Z. Huang, J. Zhu, S. Kou, X. Zhang, H. Yang, **2015**, *5*, 17773.
[34] Y.-C. Liu, J. A. Koza, J. A. Switzer, *Electrochim. Acta* **2014**, *140*, 359.
[35] Y. Y. Du, Q. Jin, J. T. Feng, N. Zhang, Y. F. He, D. Q. Li, *Catal. Sci. Technol.* **2015**, *5*, 3216.
[36] P. Li, P.-P. Huang, F.-F. Wei, Y.-B. Sun, C.-Y. Cao, W.-G. Song, *J. Mater. Chem. A* **2014**, *2*, 12739.
[37] C. Dette, M. A. Pérez-Osorio, C. S. Kley, P. Punke, C. E. Patrick, P. Jacobson, F. Giustino, S. J. Jung, K. Kern, *Nano Lett.* **2014**, *14*, 6533.
[38] G.-L. Tian, H.-B. He, J.-D. Shao, *Chin. Phys. Lett.* **2005**, *22*, 1787.
[39] H. Ünal, O. Gülseren, Ş Ellialtıoğlu, E. Mete, *Phys. Rev. B* **2014**, *89*, 205127.
[40] E. Baldini, L. Chiodo, A. Dominguez, M. Palummo, S. Moser, M. Yazdi-Rizi, G. Auböck, B. P. P. Mallett, H. Berger, A. Magrez, C. Bernhard, M. Grioni, A. Rubio, M. Chergui, *Nat. Commun.* **2017**, *8*, 13.
[41] J. M. Frost, K. L. M. Harriman, M. Murugesu, *Chem. Sci.* **2016**, *7*, 2470.
[42] Z. Liu, R. Ma, Y. Ebina, N. Iyi, K. Takada, T. Sasaki, *Langmuir* **2007**, *23*, 861.
[43] Y. Qiu, B. Lin, F. Jia, Y. Chen, B. Gao, P. Liu, *Mater. Res. Bull.* **2015**, *72*, 235.

[44] D. O. Scanlon, C. W. Dunnill, J. Buckeridge, S. A. Shevlin, A. J. Logsdail, S. M. Woodley, C. R. A. Catlow, M. J. Powell, R. G. Palgrave, I. P. Parkin, G. W. Watson, T. W. Keal, P. Sherwood, A. Walsh, A. A. Sokol, *Nat. Mater.* **2013**, *12*, 798.
[45] S. Kumar, S. T, B. Kumar, A. Baruah, V. Shanker, *J. Phys. Chem. C* **2013**, *117*, 26135.
[46] K. Das, S. N. Sharma, M. Kumar, S. K. De, *J. Phys. Chem. C* **2009**, *113*, 14783.
[47] K. Selvam, M. Swaminathan, *RSC Adv.* **2012**, *2*, 2848.
[48] G. R. Dey, A. D. Belapurkar, K. Kishore, *J. Photochem. Photobiol., A* **2004**, *163*, 503.
[49] Y. Nie, W.-N. Wang, Y. Jiang, J. Fortner, P. Biswas, *Catal. Sci. Technol.* **2016**, *6*, 6187.
[50] W. Kim, G. Yuan, B. A. McClure, H. Frei, *J. Am. Chem. Soc.* **2014**, *136*, 11034.
[51] S. Xie, Y. Wang, Q. Zhang, W. Deng, Y. Wang, *Chem. Commun.* **2015**, *51*, 3430.
[52] P. Reñones, A. Moya, F. Fresno, L. Collado, J. J. Vilatela, V. A. de la Peña O'Shea, *J. CO2 Util.* **2016**, *15*, 24.
[53] C. Gao, Q. Meng, K. Zhao, H. Yin, D. Wang, J. Guo, S. Zhao, L. Chang, M. He, Q. Li, H. Zhao, X. Huang, Y. Gao, Z. Tang, *Adv. Mater.* **2016**, *28*, 6485.
[54] Z. Q. He, D. Wang, H. Y. Fang, J. M. Chen, S. Song, *Nanoscale* **2014**, *6*, 10540.
[55] D. Wang, Y. Yu, Z. Zhang, H. Fang, J. Chen, Z. He, S. Song, *Environ. Sci. Pollut. Res.* **2016**, *23*, 18369.
[56] R. Chong, B. Wang, C. Su, D. Li, L. Mao, Z. Chang, L. Zhang, *J. Mater. Chem. A* **2017**, *5*, 8583.
[57] J. Guo, C. Mao, R. Zhang, M. Shao, M. Wei, P. Feng, *J. Mater. Chem. A* **2017**, *5*, 11016.
[58] Z. Zheng, B. Huang, X. Qin, X. Zhang, Y. Dai, *Chem. – Eur. J.* **2010**, *16*, 11266.
[59] C. M. A. Parlett, M. A. Isaacs, S. K. Beaumont, L. M. Bingham, N. S. Hondow, K. Wilson, A. F. Lee, *Nat. Mater.* **2016**, *15*, 178.

Query

Q1: Please provide the highest academic title (Dr./Prof.) for all authors, where applicable.

Q2: Please check expansion of DS for correctness.

Q3: Please provide the expansion of ICP, OES, IUPAC, INCA, TPR, TPD, HPLC, TPO, TEOA, EPSRC, HAADF, JCPDF, STEM, and LED as these have been cited once in the article.

Q4: Please define TEM, HRTEM, XPS, BJH, VB, and ACROS at the first appearance in the text.

Q5: Please check whether all equations are correctly typeset.

Q6: Please provide year of publication, volume, and page numbers in ref. (5), if now available.

Q7: Please check the appearance of (K.-I. Katsumata) in ref. (21).

Q8: Please provide publisher location in ref. (26).

Q9: Please check deletion and provide publisher location in ref. (31).

Q10: Please provide journal name in ref. (33).

Q11: Please provide surname for author's name 'S. T' in ref. (45).

Q12: Reference 58 is cited out of order. Please cite this reference in numerical order in the text.

Particle & Particle Systems Characterization

Editorial Office:
Wiley-VCH Verlag
Boschstrasse 12
69469 Weinheim, Germany

Tel.: +49 (0) 6201 606 235 or 432
Fax: +49 (0) 6201 606 500

Email: particle@wiley.com

Reprint Order Form 2017

Short DOI: ppsc. _____

Please send me and bill me for

no. of **Reprints** via ☐ airmail (+ 25 Euro)
☐ surface mail

Please send me and bill me for a

☐ **high-resolution PDF file** (330 Euro).

My Email address:

_____

Please note: It is not permitted to present the PDF file on the internet or on company homepages.

Information regarding VAT

Please note that from German sales tax point of view, the charge for **Reprints, Issues or Posters** is considered as **"supply of goods"** and therefore, in general, such delivery is a subject to German sales tax. However, this regulation has no impact on customers located outside of the European Union. Deliveries to customers outside the Community are automatically tax-exempt. Deliveries within the Community to institutional customers outside of Germany are exempted from the German tax (VAT) only if the customer provides the supplier with his/her VAT number. The VAT number (value added tax identification number) is a tax registration number used in the countries of the European Union to identify corporate entities doing business there. It starts with a country code (e.g. FR for France, GB for Great Britain) and follows by numbers.

VAT no.: _____
(Institutes / companies in EU countries only)

Purchase Order No.: _____

Delivery address / Invoice address:
Name of recipient, University, Institute, Street name and Street number, Postal Code, Country

_____
_____
_____
_____
_____
_____
_____

Date and Signature: _____

Credit Card Payment (optional) -You will receive an invoice.

VISA, MasterCard, AMERICAN EXPRESS

Please use the Credit Card Token Generator located at the website below to create a token for secure payment. The token will be used instead of your credit card number.

Credit Card Token Generator:
https://www.wiley-vch.de/editorial_production/index.php

Please transfer your token number to the space below.

Credit Card Token Number

Price list for reprints (The prices include mailing and handling charges. All Wiley-VCH prices are exclusive of VAT)

No. of pages	Price (in Euro) for orders of 50 copies	100 copies	150 copies	200 copies	300 copies	500 copies
1-4	345	395	425	445	548	752
5-8	490	573	608	636	784	1077
9-12	640	739	786	824	1016	1396
13-16	780	900	958	1004	1237	1701
17-20	930	1070	1138	1196	1489	2022
for every additional 4 pages	147	169	175	188	231	315

Wiley-VCH Verlag GmbH & Co. KGaA; Location of the Company: Weinheim, Germany;
Trade Register: Mannheim, HRB 432833, Chairman of the Board: Mark Allin
General Partner: John Wiley & Sons GmbH, Location: Weinheim, Germany
Trade Register Mannheim, HRB 432296, Managing Director: Sabine Steinbach

WILEY-VCH